

See discussions, stats, and author profiles for this publication at: <https://www.researchgate.net/publication/275361782>

3D-Printed Fluidic Devices for Nanoparticle Preparation and Flow-Injection Amperometry Using Integrated Prussian Blue Nanoparticle-Modified Electrodes

ARTICLE *in* ANALYTICAL CHEMISTRY · APRIL 2015

Impact Factor: 5.64 · DOI: 10.1021/acs.analchem.5b00903 · Source: PubMed

CITATIONS

2

READS

156

7 AUTHORS, INCLUDING:



Jennifer Satterwhite-Warden

University of Connecticut

7 PUBLICATIONS 17 CITATIONS

[SEE PROFILE](#)



Snehasis Bhakta

University of Connecticut

3 PUBLICATIONS 15 CITATIONS

[SEE PROFILE](#)



Karteek Kadimisetty

University of Connecticut

7 PUBLICATIONS 50 CITATIONS

[SEE PROFILE](#)



James Francis Rusling

University of Connecticut

218 PUBLICATIONS 9,649 CITATIONS

[SEE PROFILE](#)

3D-Printed Fluidic Devices for Nanoparticle Preparation and Flow-Injection Amperometry Using Integrated Prussian Blue Nanoparticle-Modified Electrodes

Gregory W. Bishop,[†] Jennifer E. Satterwhite,[†] Snehasis Bhakta,[†] Karteek Kadimisetty,[†] Kelsey M. Gillette,[†] Eric Chen,[†] and James F. Rusling*,^{†,‡,§,⊥}

[†]Department of Chemistry, University of Connecticut, Storrs, Connecticut 06269-3060, United States

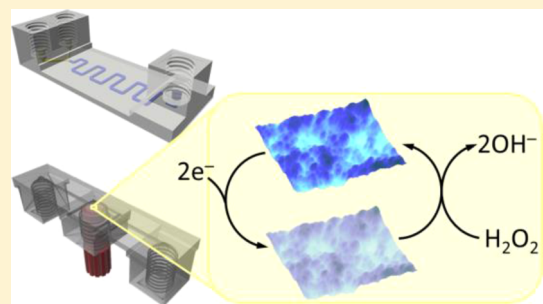
[‡]Institute of Materials Science, University of Connecticut, Storrs, Connecticut 06269-3136, United States

[§]Department of Cell Biology, University of Connecticut Health Center, Farmington, Connecticut 06030, United States

[⊥]School of Chemistry, National University of Ireland at Galway, Galway, Ireland

Supporting Information

ABSTRACT: A consumer-grade fused filament fabrication (FFF) 3D printer was used to construct fluidic devices for nanoparticle preparation and electrochemical sensing. Devices were printed using poly(ethylene terephthalate) and featured threaded ports to connect polyetheretherketone (PEEK) tubing via printed fittings prepared from acrylonitrile butadiene styrene (ABS). These devices included channels designed to have $800\text{ }\mu\text{m} \times 800\text{ }\mu\text{m}$ square cross sections and were semitransparent to allow visualization of the solution-filled channels. A 3D-printed device with a Y-shaped mixing channel was used to prepare Prussian blue nanoparticles (PBNPs) under flow rates of 100 to $2000\text{ }\mu\text{L min}^{-1}$. PBNPs were then attached to gold electrodes for hydrogen peroxide sensing. 3D-printed devices used for electrochemical measurements featured threaded access ports into which a fitting equipped with reference, counter, and PBNP-modified working electrodes could be inserted. PBNP-modified electrodes enabled amperometric detection of H_2O_2 in the 3D-printed channel by flow-injection analysis, exhibiting a detection limit of 100 nM and linear response up to $20\text{ }\mu\text{M}$. These experiments show that a consumer-grade FFF printer can be used to fabricate low-cost fluidic devices for applications similar to those that have been reported with more expensive 3D-printing methods.



Three dimensional printing or additive manufacturing has found extensive use in engineering and biotechnology.¹ The impact of 3D printing continues to grow beyond these fields with the emergence of new technologies and materials. Media coverage of 3D-printed products and devices, as well as the development of affordable, consumer-grade or desktop 3D printers have led to a groundswell of interest and inspired many new applications. Recently, 3D printers have been used to create devices for analytical applications such as electronic sensors,^{2,3} injection valves,⁴ and various accessories to help convert smartphones into portable fluorescence microscopes⁵ and instruments for performing bioassays based on fluorescence,⁶ colorimetry,⁷ and bioluminescence.⁸ 3D printing has also been employed to prepare reactionware^{9,10} and microfluidic devices^{11–22} for applications in chemical and biochemical research.

Microfluidic reactor devices¹³ with channel dimensions as small as $800\text{ }\mu\text{m}$ and centrifugal microfluidic devices¹² with capillary valves as small as $254\text{ }\mu\text{m} \times 254\text{ }\mu\text{m}$ have been prepared using 3D printers based on fused deposition modeling (FDM),¹⁵ also known as fused filament fabrication (FFF). In FFF, a thermoplastic filament is heated and forced through a nozzle to form an object using $\geq 50\text{ }\mu\text{m}$ -thick layers of extruded

polymer. Thus, resolution is limited by the diameter of the nozzle opening, which is usually 0.2 to 0.8 mm. FFF produces objects with features of $>250\text{ }\mu\text{m}$ and roughness of $\sim 8\text{ }\mu\text{m}$.¹¹ Commonly used polymer filaments for FFF include polystyrene, polycarbonate, polylactic acid, and acrylonitrile butadiene styrene.¹ However, other materials such as conductive carbon black/polymer composites have also been used.^{1,2} FFF printers can be outfitted with more than one nozzle to enable printing objects composed of multiple materials.^{2,8} Desktop FFF printers are among the most common and least expensive consumer-grade 3D printers (typically $<\$3000$). Commercially available filament can usually be obtained for $\$30$ to $\$50/\text{kg}$.

Shallan et al. recently reported the production of visibly transparent microchips with channel dimensions as small as $250\text{ }\mu\text{m}$ using a printer based on stereolithography (SLA), which relies on the polymerization of a photocurable resin by UV light.¹⁵ Microfluidic devices for fluid mixing, gradient

Received: March 6, 2015

Accepted: April 22, 2015

generation, and other applications that require optical detection were demonstrated. Desktop SLA-based printers can produce objects with resolution of $\sim 50\text{ }\mu\text{m}$ and surface roughness under 182 nm^{16} . However, uncured photopolymer or support material can be difficult to completely remove from channels with dimensions below $250\text{ }\mu\text{m}^{15}$. Even channels printed using an expensive high-resolution SLA printer exhibit surface roughness of $2.54\text{ }\mu\text{m}^{17}$. The desktop SLA-type printer employed by Shallan et al. cost \$2300, and the clear resin was \$138 for 0.5 L. Although multiple materials printing with SLA has been described,²³ difficulties associated with applying and removing multiple viscous photopolymers during a single build typically limit SLA to the production of objects composed of a single material.²⁴

Electrodes have been incorporated into 3-sided channels printed by SLA and FFF for electroanalysis and electrochemical sensing.^{25,26} Electrodes deposited on Si/SiO₂ substrates or embedded in epoxy were positioned in the open side of SLA-printed channels.²⁵ The flow cell assembly, which was bound together using cotton thread, enabled linear sweep voltammetry with a two-electrode system for flow rates up to 64 mL min^{-1} . FFF-printed channels were sealed with a transparent plastic film, and 0.5 mm diameter carbon and Pt electrodes were incorporated into channels for electrochemical biosensing of a virus labeled with CdS quantum dots by differential pulse voltammetry of Cd²⁺.²⁶

PolyJet and MultiJet 3D-printing technologies combine inkjet printing of liquid photopolymer with instant UV curing to build objects from layers as thin as $16\text{ }\mu\text{m}^1$. Due to the smooth surfaces produced by these techniques and the availability of clear photopolymer materials, transparent objects, including transparent microfluidic devices, can be prepared. However, as with SLA, support material can be difficult to remove from small channels. Spence et al. utilized a 3D printer based on PolyJet technology to prepare transparent microfluidic devices with channel dimensions as small as $500\text{ }\mu\text{m}^{18-20}$. These devices feature threaded ports that enable the reversible integration of external devices like membrane inserts and electrodes for drug transport studies, cell viability assays, and electrochemical sensing. Modular microfluidic devices have been also been prepared using these methods.^{21,22} Device modules can be connected using rubber O-rings²¹ or designed to directly connect similar to Lego bricks²² for assembly of customized and integrated microfluidic devices. However, printers based on PolyJet and MultiJet technologies typically cost 10 to 100 times desktop FDM and SLA printers^{1,16} and require materials of proprietary composition that cost $\sim \$300/\text{kg}$.

Mail-order services are available that allow customers to upload design files and obtain corresponding objects printed using high-resolution 3D printers.^{17,21,22} These services can be very useful for startup companies trying to develop new products and low-production markets where large initial investments in infrastructure required for plastic molding technologies are not feasible.¹⁷ However, even a small microfluidic device with overall dimensions of tens of millimeters can cost $\sim \$200$ using a service of this type.

Researchers continue to push the boundaries of 3D printing by developing new systems and materials for applications for custom 3D-printing applications. Lewis et al. have demonstrated 3D printing of various custom materials by interfacing micropositioning stages with pneumatic fluid delivery systems.²⁷⁻²⁹ These techniques have been used to prepare

microstructured Li-ion batteries from nanoparticle suspensions,²⁷ lightweight cellular composites from epoxy-based inks,²⁸ and strain sensors embedded within elastomers by extruding conductive carbon grease directly into a silicone elastomer.²⁹

With respect to commercially available desktop 3D printers, while SLA printers offer the ability to produce inexpensive transparent microfluidic devices with superior roughness, FFF printers use less expensive materials and are capable of printing objects composed of multiple materials. Here, we demonstrate that a desktop FFF printer can be used to prepare semitransparent functional fluidic devices that feature channels with dimensions as small as $250\text{ }\mu\text{m}$. While previously reported microfluidic devices produced by FFF have been mostly opaque due to the material used,¹⁵ we employ a clear poly(ethylene terephthalate) (PET) filament to prepare devices that are transparent enough to enable observation of dye solutions in the printed channels. We show that a 3D-printed Y-mixing channel can be used to prepare Prussian blue nanoparticles. We also demonstrate that FFF, like PolyJet,²⁰ can be used to construct fluidic devices with ports to incorporate electrodes for electrochemical measurements. Specifically, we develop electrochemical sensors for hydrogen peroxide based on Prussian blue nanoparticle-modified electrodes integrated into 3D-printed fluidic channels.

MATERIALS AND METHODS

Materials. 1.75 mm diameter PET and ABS filaments for 3D printing were obtained from MadeSolid (Oakland, CA, USA) and MakerBot (Brooklyn, NY, USA), respectively. Au (0.1 mm and 0.5 mm dia.), Pt (0.25 mm dia.), and Ag (0.5 mm dia.) wires as well as potassium ferricyanide, iron(II) chloride, sodium phosphate dibasic, N-(3-(dimethylamino)propyl)-N'-ethylcarbodiimide hydrochloride (EDC), n-hydroxysulfosuccinimide (NHSS) sodium salt, sulfuric acid (98.0%), chitosan (Mw 60,000–120,000), and poly(diallyldimethylammonium chloride) (Mw 200,000–300,000; 20% in water) were obtained from Sigma-Aldrich (St. Louis, MO, USA). NaCl, KCl, and acetic acid were purchased from J.T. Baker (Center Valley, PA, USA). Citric acid monohydrate, potassium phosphate monobasic, and hydrogen peroxide (30% solution) were obtained from Fisher Scientific (Pittsburgh, PA). All solutions were prepared using $18\text{ M}\Omega\cdot\text{cm}$ water purified by passing house-distilled water through a Hydro Service and Supplies purification system (Durham, NC, USA).

3D-printed fluidic device preparation. Fluidic devices were designed using 123D Design software (Autodesk, San Rafael, CA, USA). Design files were converted into printer instructions by the MakerWare slicer program (MakerBot). Threaded ports in the fluidic devices and threaded fittings were designed by modifying open-source threaded nut and screw design files.³⁰ Fluidic devices were fabricated using a Replicator 2X desktop 3D printer (MakerBot).

Fluidic devices were printed using clear PET filament, and threaded fittings were printed using natural ABS. Threaded fittings were interfaced with polyetheretherketone (PEEK) tubing and ethylene tetrafluoroethylene (ETFE) ferrules (Upchurch Scientific, Oak Harbor, WA, USA) to provide access to the fluidic channels. Images of 3D-printed devices were obtained using a Firefly GT800 microscope (Belmont, MA, USA). Surface roughness of top and bottom layers of printed devices were investigated using a Dektak 150 surface

profiler (Plainview, NY, USA) equipped with a 5 μm diameter stylus. Scan length was 2.5 mm. Scan duration was 200 s.

Nanoparticle formation in a 3D-printed Y-shaped mixing channel. A 3D-printed Y-shaped mixing channel was interfaced with a Harvard Apparatus Pump 33 dual syringe pump (Holliston, MA) to prepare Prussian blue nanoparticles (PBNPs) by mixing iron(II) chloride and potassium ferricyanide solutions by slight modification of published protocols based on conventional mixing.^{31,32} Citrate-coated PBNPs (citrate-PBNPs) were formed by mixing 5 mM iron(II) chloride in 25 mM citric acid and 5 mM potassium ferricyanide in 25 mM citric acid.³¹ PBNPs coated with PDDA and chitosan (PDDA-PBNPs-CS) were prepared by mixing 10 mM potassium ferricyanide with 10 mM iron(II) chloride in 1.6% acetic acid that also contained 0.64% PDDA and 0.24% chitosan.³²

Particle sizes were determined by atomic force microscopy (AFM) using a Veeco Multimode AFM with a Digital Instruments Nanoscope IV controller (Santa Barbara, CA, USA). PBNP suspensions were diluted 100x in purified water and deposited on mica discs. AFM was operated in tapping mode using a symmetric tip high-resolution probe (MPP-11100, Bruker AFM Probes, Camarillo, CA, USA). Hydrodynamic radii were measured by dynamic light scattering using an ALV/LSE-5004 (Langen, Germany), and particle zeta potentials were ascertained using a ZetaPlus analyzer (Brookhaven Instruments Corporation, Holtsville, NY, USA).

Electrode fabrication. Disk electrodes were fabricated from 5 to 10 mm long Au, Ag, and Pt wires that were 0.1, 0.25, or 0.5 mm in diameter. Metal wires were inserted into PEEK tubing of 0.02 in internal diameter (Upchurch Scientific) for insulation. One end of each wire was connected to 24-gauge copper wire by soldering or through use of Ag/AgCl paste (Gwent, Pontypool, UK) to provide contacts for electrochemical measurements.

Working, counter, and reference PEEK-tubing-insulated disk electrodes were grouped together and inserted into an opening of a threaded, 3D-printed ABS fitting. Gaps between fittings and electrodes were filled with epoxy. Electrodes were polished using 600 grit abrasive paper (Buehler, Lake Bluff, IL, USA). Ag electrodes were coated with AgCl using a 9 V battery and a 2.2 M Ω resistor to supply $\sim 4 \mu\text{A}$ to the Ag anode, which was immersed in a 3.5 M KCl solution along with an Ag/AgCl cathode.

For flow-injection analysis of H₂O₂, Au working electrodes were first cycled 20 times from -0.2 to +1.4 V vs Ag/AgCl in 0.5 M sulfuric acid at 100 mV s⁻¹ to remove surface oxides. Surface areas of Au electrodes were determined by integrating the gold oxide reduction peaks as described previously.^{33,34} Au electrodes were subsequently coated with 4 mM 3-mercaptopropionic acid in ethanol to provide surface carboxylate groups.³⁵ After washing with ethanol and purified water, a layer-by-layer assembly of PDDA (2 mg mL⁻¹ in 0.05 M NaCl) and citrate-coated PBNPs was formed on the carboxylate-modified Au electrodes by successively drop-casting these reagents for 20 min each. Alternatively, PBNPs coated with PDDA and chitosan were deposited on carboxylate-functionalized Au electrodes by first activating carboxylate groups using a 200 mM EDC and 400 mM NHSS solution for 10 min.³⁶ PBNPs coated with PDDA and chitosan were then drop-casted on the electrodes to form amide bonds between activated carboxylate groups and amine groups of chitosan.

AFM was used to investigate nanostructured surfaces of PBNP-modified Au electrodes. One mm-long sections of polished Au wire (0.5 mm dia.) encased in PEEK tubing were adhered to AFM sample pucks using double-sided tape. Au disks were modified with citrate-PBNPs and PDDA-PBNPs-CS as described above.

Electrochemical measurements. Electrochemical measurements were performed using a CH Instruments 1232 bipotentiostat (Austin, TX, USA). Flow-injection amperometry was conducted using 3D-printed fluidic devices with integrated electrodes that were placed downstream of a Harvard Apparatus Pump 11 Elite syringe pump and a Rheodyne 9725 injector valve (Rohnert Park, CA) equipped with a 50 μL sample loop. Since electrode surface areas for different Au working electrodes of the same nominal diameter (0.1 mm) varied by 15% as determined from gold oxide reduction measurements, amperometric response was normalized by electrode surface area and expressed as current density.

RESULTS

Semitransparent channels prepared by FFF. PET devices with fluidic channels were printed and filled with 1 mM methylene blue in 10 mM phosphate buffered saline (PBS, pH 7.4) through 3 mm diameter access holes on the top of the device (Figure 1A). Channels with square cross sections (800

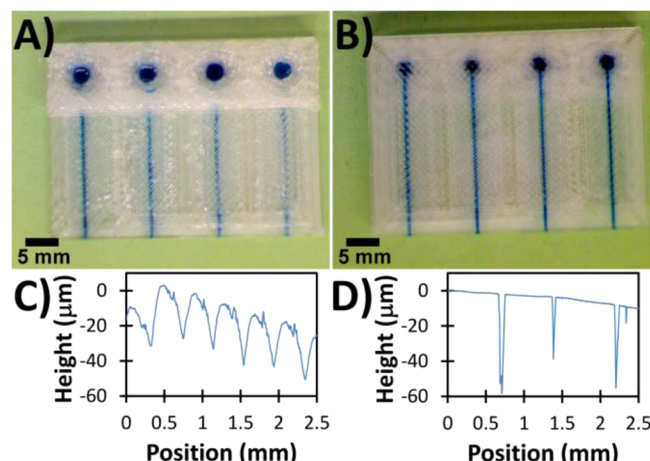


Figure 1. Semitransparent 3D-printed PET channels filled with 1 mM methylene blue solution for visualization. (A) Top view of 800 $\mu\text{m} \times 800 \mu\text{m}$ square cross-sectional channels with top sides of channels designed to be (from left to right) 200, 400, 600, and 800 μm from the top side of the device. 3 mm access holes are printed in a 10.5 mm wide section at the top of the device. (B) Bottom view of the same channels depicted in part A with the bottom sides of the channels designed to be 800, 600, 400, and 200 μm from the bottom side of the device. Surface profile traces of (C) the top and (D) bottom sides of the printed devices obtained using a stylus profilometer.

$\mu\text{m} \times 800 \mu\text{m}$) were designed and printed such that the bottom and top boundaries of each channel were 200–800 μm from the bottom and top layers of the device, respectively (Figure 1). The access holes on the top of the device are printed in a 10.5 mm wide section that is 4.4 mm high, thereby extending 2.8 to 3.4 mm above the top of the channels. Because the devices are formed from 200 μm -thick layers of thin ribbons of heated PET filament, objects printed by FFF are not completely transparent; however, dye solution can be observed in the printed channels through at least four layers (800 μm) of the printed

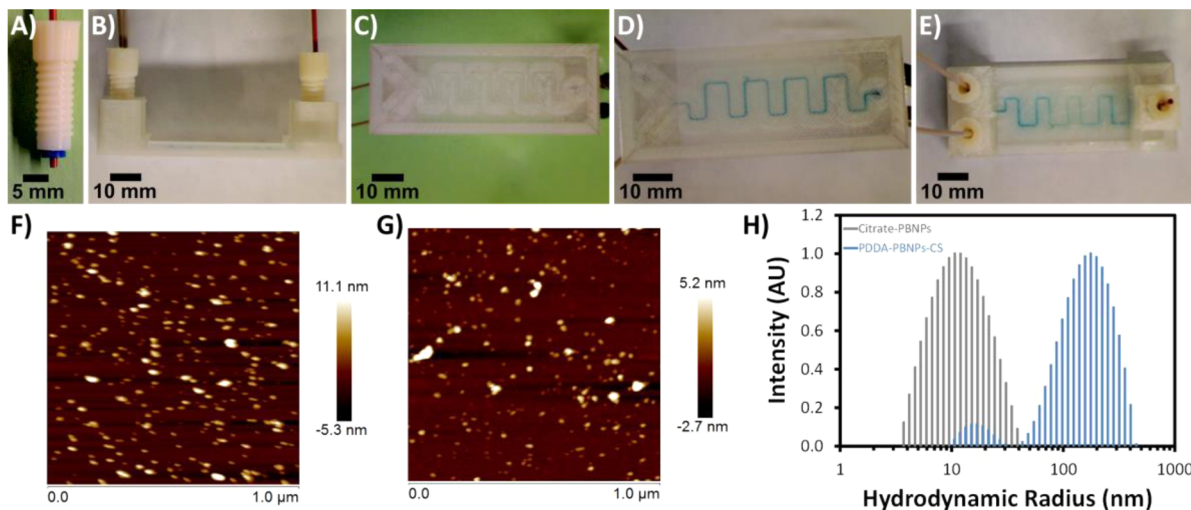


Figure 2. Preparation of Prussian blue nanoparticles (PBNNPs) using a 3D-printed Y-shaped mixing device. Images of (A) a 3D-printed ABS fitting, (B) side view of the device, (C and D) bottom views of the device (C) before and (D) after mixing 5 mM iron(II) chloride and 5 mM potassium ferricyanide solutions to form citrate-PBNNPs, and (E) top view of citrate-PBNNP-filled device. AFM images of (F) citrate-PBNNPs and (G) PDDA-PBNNPs-CS deposited on mica. (H) Dynamic light scattering results for hydrodynamic radii of citrate-PBNNPs and PDDA-PBNNPs-CS formed using flow rates of 2000 $\mu\text{L min}^{-1}$.

filament (Figure 1). Dye solution is completely obscured when viewed through 14 or more layers near the access holes (Figure 1A).

The bottom side of the device (Figure 1B) is more transparent than the top side (Figure 1A) as evidenced by visualization of dye solution in the channels. Profilometry shows the top layer to consist of a repeating, rough peak-and-valley structures (Figure 1C) that are attributed to adjacent cylindrical threads of PET that comprise each layer. The average separation distance for the valleys between the peak-shaped structures on the top layer is 400 (± 13) μm , which is consistent with the opening diameter of the 3D printer extruder nozzle (400 μm). The bottom layer of the device is printed against the flat, heated surface of the build plate, thus minimizing surface roughness (Figure 1D) and improving the visualization of the dye solution in the channels (Figure 1B). Printed channel widths were $\sim 32\%$ smaller than design widths, and printed heights were approximately the same as design heights (Figure S1, Supporting Information). Channels with dimensions as small as 250 μm were printed, and the dual extrusion design of the printer also enabled printing single devices from two materials to produce channels in hybrid PET/ABS devices (Figure S2, Supporting Information).

Preparation of Prussian blue nanoparticles in a 3D-printed Y-shaped channel. A Y-shaped channel (Figure 2) was used to facilitate the formation of Prussian blue nanoparticles (PBNNPs) by mixing solutions containing iron(II) chloride and potassium ferricyanide that were delivered to the channel via a dual syringe pump. Both citrate-modified PBNNPs (citrate-PBNNPs) and PBNNPs modified with PDDA and chitosan (PDDA-PBNNPs-CS) were separately prepared in the Y-shaped mixing device. The device features threaded access ports to facilitate fluidic delivery through PEEK tubing inserted in threaded, 3D-printed ABS fittings (Figure 2A). Channels were designed to be 800 $\mu\text{m} \times 800 \mu\text{m}$ with a total volume of 93 μL . Solutions were mixed using flow rates of 100 to 2000 $\mu\text{L min}^{-1}$ with no leakage at the inlet and outlet ports or in the channel.

Due to the semitransparent nature of the 3D-printed PET mixing device, Prussian blue formation could be visualized in

the channel (Figure 2D,E). Particle sizes measured from AFM images (Figure 2F,G) were 9 (± 3) nm for citrate-PBNNPs and 4 (± 1) nm for PDDA-PBNNPs-CS, which are comparable to analogous PBNNPs prepared by conventional stirring.^{31,32} Citrate-PBNNPs exhibited an average hydrodynamic radius of 12 (± 4.7) nm, which is also consistent with values reported for citrate-PBNNPs obtained using conventional mixing.³¹ In contrast, PDDA-PBNNPs-CS prepared in the Y-shaped channel exhibited a bimodal distribution of hydrodynamic radii with minor node of 17 (± 3.5) nm and major node of 180 (± 82) nm, suggesting the formation of larger agglomerates. Zeta potentials of citrate-PBNNPs and PDDA-PBNNPs-CS were found to be -26 (± 3.8) mV and $+57$ (± 1.0) mV, respectively.

3D-printed fluidic devices with integrated electrodes for amperometric detection of H_2O_2 via flow-injection analysis. Prussian blue has been shown to exhibit electrocatalytic behavior toward the reduction of H_2O_2 .³⁷ 3D-printed fluidic devices with Prussian blue nanoparticle (PBNNP)-modified Au electrodes (0.1 mm dia.) were used for amperometric detection of H_2O_2 via flow-injection analysis. Electrodes were incorporated into 3D-printed fluidic devices through a threaded port in the center (Figure 3) in a manner like that which was recently reported by Erkal et al., who used a 3D printer based on PolyJet technology.²⁰

3D-printed ABS fittings (Figure 3A) equipped with disk electrodes (Figure 3B,C) were used to perform electrochemical measurements in a 3D printed channel designed to be 800 $\mu\text{m} \times 800 \mu\text{m} \times 56 \text{ mm}$. The electrodes were able to access the solution through a 6.6 mm diameter opening in the center of the channel (Figure 3E), and the total volume of the channel (including electrode access opening) was 79 μL . Electrochemical responses of electrodes incorporated in 3D-printed channels were identical to those obtained from electrodes immersed in solutions (Figure S3, Supporting Information).

Au working electrodes were modified with citrate-PBNNPs or PDDA-PBNNPs-CS as described previously in the Materials and Methods section. AFM images (Figure 4A–C) show the nanostructured surfaces of citrate-PBNNP- and PDDA-PBNNP-CS-modified Au electrodes. Both citrate-PBNNP- and PDDA-

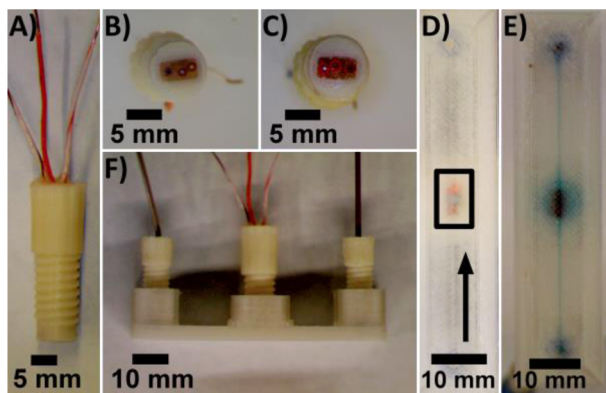


Figure 3. 3D-printed device with electrodes incorporated in the fluidic channel. (A) Side view of a threaded ABS fitting with integrated electrodes. (B and C) Bottom views of ABS fittings equipped with (B) 0.5 mm Ag/AgCl reference, 0.25 mm Pt working, and 0.5 mm Au counter electrodes and with (C) 0.25 mm Pt counter, 0.1 mm Au working, and 0.5 mm Ag/AgCl reference electrodes. (D) Bottom view of a 3D-printed PET device with reference, working, and counter electrodes (in box, bottom to top) incorporated in the fluidic channel. Arrow indicates direction of flow. (E and F) Bottom (E) and side (F) views of device filled with 0.1 mM methylene blue in 10 mM PBS, pH 7.4.

PBNP-CS-modified electrodes produced a pair of well-defined peaks attributed to the Prussian blue/Prussian white redox couple (Figure 4D,E).³⁷ Addition of H₂O₂ to the electrolyte solution (10 mM PBS, pH 7.4) resulted in an increase in cathodic current that is associated with the electrocatalytic reduction of H₂O₂ by Prussian blue. When exposed to H₂O₂, the background-corrected cathodic peak current for the PDDA-PBNP-CS-modified electrode increased by 18.8% (Figure 4E). PDDA-PBNP-CS-modified electrodes were superior to citrate-PBNP-modified electrodes as evidenced by their larger CV responses.

Flow-injection amperometric detection of H₂O₂ was carried out in the 3D-printed fluidic device using a flow rate of 100 μ L

min⁻¹ with PDDA-PBNP-CS-modified Au working electrodes held at a potential of -0.1 V vs Ag/AgCl. Peak-shaped responses (Figure 5A) from standards in 10 mM PBS (pH 7.4) increased with increasing H₂O₂ concentration, and the detection limit was 100 nM (S/N = 3). Responses from different electrodes under the same conditions differed by 6.3%. A linear relationship between peak current signal and H₂O₂ concentration was obtained for 100 nM to 20 μ M (Figure 5B).

■ DISCUSSION

In FFF, objects are built by extruding thin ribbons of a thermoplastic filament through a heated nozzle. Since each layer of the object is composed of cylindrical threads of thermoplastic and the object comprises many layers, objects fabricated by FFF lack transparency, even when a clear thermoplastic filament is used. However, semitransparent fluidic devices can be produced by FFF to allow visualization of solutions within channels as small as ~250 μ m (SI, Figure S1). Visualization of solutions within channels can be improved by minimizing the number of layers in the design and by printing the bottom layer of the device on a flat, heated platform, which leads to a smooth surface through which solutions within channels can be better viewed. Since FFF-type printers can be easily outfitted with multiple extruders, multimaterial printing is also possible (SI, Figure S2).^{2,8}

As with 3D-printed fluidic devices prepared by PolyJet and SLA, fluidic devices fabricated using FFF can be designed to feature threaded ports that allow access to the channels for fluid delivery and electrochemical measurements. However, the lower material cost associated with FFF can make it an attractive alternative to PolyJet and SLA technologies. The fluidic devices demonstrated here each took less than 50 min to print and required \$0.30 to \$0.60 in material. FFF can also be used to prepare fluidic devices for a modular approach to electrochemical measurements in a fashion following that which was recently reported by Erkal et al.²⁰ using a PolyJet-based printer. Here, we demonstrated H₂O₂ sensing based on

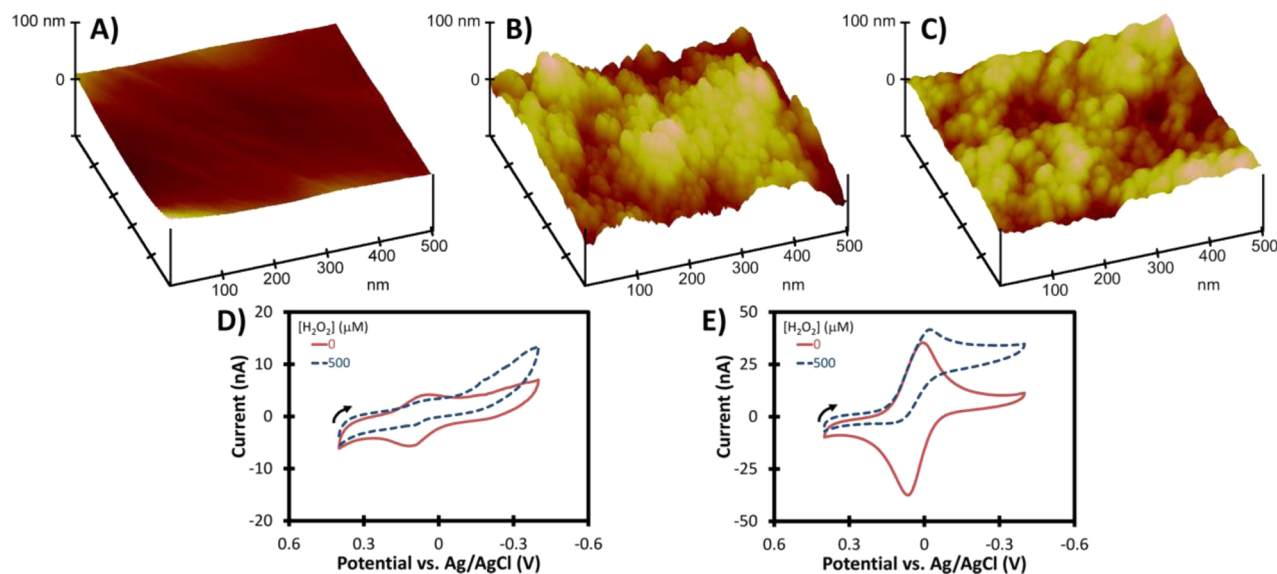


Figure 4. Gold disk electrodes modified with PBNPs. AFM images of (A) an Au disk, (B) a citrate-PBNP-modified Au disk, and (C) a PDDA-PBNP-CS-modified Au disk. Cyclic voltammograms of (D) citrate-PBNP- and (E) PDDA-PBNP-CS-modified Au electrodes (0.1 mm diameter) in 10 mM PBS, pH 7.4 in the absence and presence of 500 μ M H₂O₂ (scan rate = 25 mV s⁻¹). Arrows indicate direction of scans.

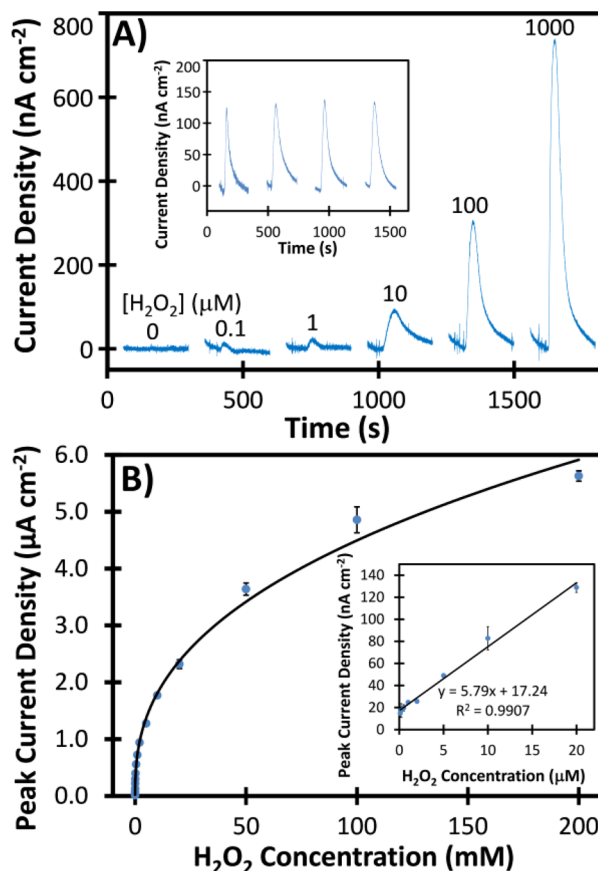


Figure 5. Flow-injection amperometric detection of H₂O₂ in 10 mM PBS using a 3D-printed fluidic device with integrated PDDA-PBNP-CS-modified Au electrodes. (A) Representative peak-shaped amperometric responses obtained by injecting 0 to 1 mM H₂O₂ at a flow rate of 100 $\mu\text{L min}^{-1}$ and an applied potential of −0.1 V vs Ag/AgCl. Inset shows responses for 20 μM H₂O₂ using four different PDDA-PBNP-CS-modified Au electrodes under the same conditions. (B) Calibration curve for amperometric data. Inset shows the linear portion of the calibration curve from 0.1 to 20 μM . Error bars correspond to one standard deviation for average responses from three injections using the same PDDA-PBNP-CS-modified Au electrode.

Prussian blue nanoparticle-modified electrodes incorporated into 3D-printed channels.

There has been a considerable amount of attention placed on developing improved electrochemical strategies for detecting H₂O₂ with a few methods based on different nanomaterial composites boasting detection limits in the low nM to pM range.^{37–41} Thanks to its sensitivity and selectivity toward the electrocatalytic reduction of H₂O₂, Prussian blue is an attractive material for sensing applications and has been regarded as an “artificial enzyme peroxidase”.³⁹ The low-potential requirement for electrocatalytic reduction of H₂O₂ by PBNPs helps reduce background signal from the reduction of oxygen and other potential interfering species.³⁷ PBNPs are also easy to prepare and exhibit good stability.

Here, PBNPs with two different surface modifications were produced using a 3D-printed Y-shaped mixing channel, and PBNP-modified electrodes were incorporated into 3D-printed channels for detection of H₂O₂. This simple, inexpensive amperometric sensing method displayed a linear response for 0.1 to 20 μM H₂O₂ and detection limit of 100 nM, which are comparable to other nanomaterials-based electrochemical

sensing strategies for H₂O₂.³⁸ 3D-printed fluidic devices and electrode fittings were reusable, and responses from different PBNP-modified electrodes under the same experimental conditions for H₂O₂ detection differed by 6.3%.

Due to the design of the fluidic device, which includes a threaded port, and ease of fabrication of electrode fittings, different types of electrodes or electrode arrays can be incorporated into the channel for other electrochemical sensing applications. The limited visibility of electrodes in the channel through the 3D-printed layers may impede sensing strategies based on optical signals like electrochemiluminescence. However, optical detection methods may also be possible in FDM-printed devices if optical fibers⁴² can be used in place of or in conjunction with electrodes. Reducing the number of 3D-printed layers separating the signal transducer and the viewing window, while maintaining channel integrity to avoid leaking, may also help enable detection strategies based on optical methods. For the 3D-printed fluidic devices described here, no leaking was observed at the inlet/outlet ports or in the channel with flow rates as high as 2000 $\mu\text{L min}^{-1}$, the maximum flow rate that was tested in these studies. The low-cost, easy-to-fabricate 3D-printed fluidic devices, electrode fittings, and PBNP-modified electrodes presented here have the potential to serve as platforms for simple, adaptable biosensing strategies.

CONCLUSIONS

The materials used in FFF-type printers are typically lower in cost than either of those used in printers based on SLA or PolyJet 3D-printing technologies. Furthermore, consumer-grade FFF printers are similar or lower in cost than desktop SLA printers, are 10–100 times less expensive than PolyJet printers, and can easily be outfitted to print objects composed of multiple materials. Though FFF lacks the printing resolution of SLA and PolyJet technologies, here we show that FFF can still be used to prepare semitransparent fluidic devices for analytical applications. Fluidic devices with threaded ports were printed to enable integration of commercially available tubing as well as specially designed 3D-printed fittings that feature electrodes. Prussian blue nanoparticles were prepared in a 3D-printed mixing channel and applied to electrode surfaces for H₂O₂ sensing via flow-injection amperometry in 3D-printed fluidic devices. FFF offers a low-cost, simple solution to prototyping and production of fluidic devices and sensors.

ASSOCIATED CONTENT

Supporting Information

Channel size measurement, comparison of electrochemical responses obtained inside and outside 3D-printed channels, and dual-material-printed ABS/PET fluidic devices. The Supporting Information is available free of charge on the ACS Publications website at DOI: 10.1021/acs.analchem.5b00903.

AUTHOR INFORMATION

Corresponding Author

*Tel.: +1 860 486 4909. Fax: +1 860 486 2981. E-mail: james.rusling@uconn.edu.

Notes

The authors declare no competing financial interest.

ACKNOWLEDGMENTS

This work was supported by grant EB014586 from the National Institute of Biomedical Imaging and Bioengineering (NIBIB) at

the National Institutes of Health. K.M.G. acknowledges support from the University of Connecticut Research Experiences for Undergraduates (REU) Program of the National Science Foundation under award number CHE-1062946. The authors thank Nhi M. Doan and Fotios Papadimitrakopoulos for their assistance with surface profilometry.

■ REFERENCES

- (1) Gross, B. C.; Erkal, J. L.; Lockwood, S. Y.; Chen, C.; Spence, D. M. *Anal. Chem.* **2014**, *86*, 3240–3253.
- (2) Leigh, S. J.; Bradley, R. J.; Purssell, C. P.; Billson, D. R.; Hutchins, D. A. *PLoS One* **2012**, *7*, e49365.
- (3) Salvo, P.; Raedt, R.; Carrette, E.; Schaubroeck, D.; Vanfleteren, J.; Cardon, L. *Sensor. Actuat. A-Phys.* **2012**, *174*, 96–102.
- (4) Su, C.-K.; Hsia, S.-C.; Sun, Y.-C. *Anal. Chim. Acta* **2014**, *838*, 58–63.
- (5) Wei, Q.; Qi, H.; Luo, W.; Tseng, D.; Ki, S. J.; Wan, Z.; Göröcs, Z.; Bentolila, L. A.; Wu, T.-T.; Sun, R.; Ozcan, A. *ACS Nano* **2013**, *7*, 9147–9155.
- (6) Coskun, A. F.; Nagi, R.; Sadeghi, K.; Phillips, S.; Ozcan, A. *Lab Chip* **2013**, *13*, 4231–4238.
- (7) Coskun, A. F.; Wong, J.; Khodadadi, D.; Nagi, R.; Tey, A.; Ozcan, A. *Lab Chip* **2013**, *13*, 636–640.
- (8) Roda, A.; Michelini, E.; Cevenini, L.; Calabria, D.; Calabretta, M. M.; Simoni, P. *Anal. Chem.* **2014**, *86*, 7299–7304.
- (9) Symes, M. D.; Kitson, P. J.; Yan, J.; Richmond, C. J.; Cooper, G. J. T.; Bowman, R. W.; Vilbrandt, T.; Cronin, L. *Nat. Chem.* **2012**, *4*, 349–354.
- (10) Kitson, P. J.; Symes, M. D.; Dragone, V.; Cronin, L. *Chem. Sci.* **2013**, *4*, 3099–3103.
- (11) McDonald, J. C.; Chabinyc, M. L.; Metallo, S.; Anderson, J. R.; Stroock, A. D.; Whitesides, G. M. *Anal. Chem.* **2002**, *74*, 1537–1545.
- (12) Moore, J. L.; McCuiston, A.; Mittendorf, I.; Ottway, R.; Johnson, R. D. *Microfluid. Nanofluid.* **2011**, *10*, 877–888.
- (13) Kitson, P. J.; Rosnes, M. H.; Sans, V.; Dragone, V.; Cronin, L. *Lab Chip* **2012**, *12*, 3267–3271.
- (14) Chisholm, G.; Kitson, P. J.; Kirkaldy, N. D.; Bloor, L. G.; Cronin, L. *Energy Environ. Sci.* **2014**, *7*, 3026–3032.
- (15) Shallan, A. I.; Smejkal, P.; Corban, M.; Guijt, R. M.; Breadmore, M. C. *Anal. Chem.* **2014**, *86*, 3124–3130.
- (16) Comina, G.; Suska, A.; Filippini, D. *Lab Chip* **2014**, *14*, 2978–2982.
- (17) Au, A. K.; Lee, W.; Folch, A. *Lab Chip* **2014**, *14*, 1294–1301.
- (18) Anderson, K. B.; Lockwood, S. Y.; Martin, R. S.; Spence, D. M. *Anal. Chem.* **2013**, *85*, 5622–5626.
- (19) Chen, C.; Wang, Y.; Lockwood, S. Y.; Spence, D. M. *Analyst* **2014**, *139*, 3219–3226.
- (20) Erkal, J. L.; Selimovic, A.; Gross, B. C.; Lockwood, S. Y.; Walton, E. L.; McNamara, S.; Martin, R. S.; Spence, D. M. *Lab Chip* **2014**, *14*, 2023–2032.
- (21) Lee, K. G.; Park, K. J.; Seok, S.; Shin, S.; Kim, D. H.; Park, J. Y.; Heo, Y. S.; Lee, S. J.; Lee, T. J. *RSC Adv.* **2014**, *4*, 32876–32880.
- (22) Bharghava, K. C.; Thompson, B.; Malmstadt, N. *Proc. Natl. Acad. Sci. U.S.A.* **2014**, *111*, 15013–15018.
- (23) Choi, J.-W.; Kim, H.-C.; Wicker, R. J. *Mater. Process. Technol.* **2011**, *211*, 318–328.
- (24) Wicker, R.; MacDonald, E. W. *Virtual Phys. Prototyp.* **2012**, *7*, 181–194.
- (25) Snowden, M. E.; King, P. H.; Covington, J. A.; Macpherson, J. V.; Unwin, P. R. *Anal. Chem.* **2010**, *82*, 3124–3131.
- (26) Krejcova, L.; Nejdl, L.; Rodrigo, M. A. M.; Zurek, M.; Matousek, M.; Hynek, D.; Zitka, O.; Kopel, P.; Adam, V.; Kizek, R. *Biosens. Bioelectron.* **2014**, *54*, 421–427.
- (27) Sun, K.; Wei, T.-S.; Ahn, B. Y.; Seo, J. Y.; Dillon, S. J.; Lewis, J. A. *Adv. Mater.* **2013**, *25*, 4539–4543.
- (28) Compton, B. G.; Lewis, J. A. *Adv. Mater.* **2014**, *26*, 5930–5935.
- (29) Muth, J. T.; Vogt, D. M.; Truby, R. L.; Mengüç, T.; Kolesky, D. B.; Wood, R. J.; Lewis, J. A. *Adv. Mater.* **2014**, *26*, 6307–6312.
- (30) Sneakypoo, R. *Fully Printable PCB Vise*. <http://www.thingiverse.com/thing:21357> (accessed May 8, 2014).
- (31) Shokouhimehr, M.; Soehnlen, E. S.; Hao, J.; Griswold, M.; Flask, C.; Fan, X.; Basilon, J. P.; Basu, S.; Huang, S. D. *J. Mater. Chem.* **2010**, *20*, 5251–5259.
- (32) Chen, S.; Yuan, R.; Chai, Y.; Xu, Y.; Min, L.; Li, N. *Sens. Actuat. B-Chem.* **2008**, *135*, 236–244.
- (33) Trasatti, S.; Petrii, O. A. *Pure Appl. Chem.* **1991**, *63*, 711–734.
- (34) Krause, C. E.; Otieno, B. A.; Latus, A.; Faria, R. C.; Patel, V.; Gutkind, J. S.; Rusling, J. F. *ChemistryOpen* **2013**, *2*, 141–145.
- (35) Chikkaveeraiah, B. V.; Liu, H.; Mani, V.; Papadimitrakopoulos, F.; Rusling, J. F. *Electrochem. Commun.* **2009**, *11*, 819–822.
- (36) Mani, V.; Chikkaveeraiah, B. V.; Patel, V.; Gutkind, J. S.; Rusling, J. F. *ACS Nano* **2009**, *3*, 585–594.
- (37) Karyakin, A. A. *Electroanalysis* **2001**, *13*, 813–819.
- (38) Chen, S.; Yuan, R.; Chai, Y.; Hu, F. *Microchim. Acta* **2013**, *180*, 15–32.
- (39) Karyakin, A. A.; Puganova, E. A.; Budashov, I. A.; Kurochkin, I. N.; Karyakina, E. E.; Levchenko, V. A.; Matveyenko, V. N.; Varfolomeyev, S. D. *Anal. Chem.* **2004**, *76*, 474–478.
- (40) Lu, X.; Li, Y.; Zhang, X.; Du, J.; Zhou, X.; Xue, Z.; Liu, X. *Anal. Chim. Acta* **2012**, *711*, 40–45.
- (41) Zhiguo, G.; Shuping, Y.; Zaijun, L.; Xiulan, S.; Guangli, W.; Yinjun, F.; Junkang, L. *Anal. Chim. Acta* **2011**, *701*, 75–80.
- (42) Wang, X.-D.; Wolfbeis, O. S. *Anal. Chem.* **2013**, *85*, 487–508.